Uncertainty in Remote Sensing of Streams using Noncontact Radars

Mushfiqur Rahman Khan, Jonathan Gourley, Jorge Duarte, Humberto Vergara, Daniel Wasielewski, Pierre-Alain Ayral, John Fulton

Journal of Hydrology 603 (2021) 126809

Contents lists available at ScienceDirect

Journal of Hydrology

journal homepage: www.elsevier.com/locate/jhydrol

Research papers

Uncertainty in remote sensing of streams using noncontact radars

Mushfiqur Rahman Khan [a,b], Jonathan J. Gourley [c,*], Jorge A. Duarte [b,c], Humberto Vergara [b,c], Daniel Wasielewski [c], Pierre-Alain Ayral [d], John W. Fulton [e]

[a] School of Civil Engineering and Environmental Science, University of Oklahoma, Norman, OK, USA
[b] Cooperative Institute for Mesoscale Meteorological Studies, University of Oklahoma, Norman, OK, USA
[c] NOAA/National Severe Storms Laboratory, Norman OK, USA
[d] Hydrosciences Montpellier, Univ. Montpellier, IMT Mines Ales, IRD, CNRS, Ales, France
[e] U.S. Geological Survey, Denver, CO, USA

ARTICLE INFO

This manuscript was handled by Emmanouil Anagnostou, Editor-in-Chief with the assistance of Jesús Mateo Lázaro, Associate Editor

Keywords:
Flash floods
Noncontact streamgauging
Remote sensing
Uncertainty estimation

ABSTRACT

Accounting for freshwater resources and monitoring floods are vital functions for societies throughout the world. Remote-sensing methods offer great prospects to expand stream monitoring in developing countries and to smaller, headwater streams that are largely ungauged worldwide. This study evaluates the potential to estimate discharge using eight radar units that have been installed over streams in diverse hydrologic and hydraulic settings across the United States. The research highlights error characteristics associated with the measurements of stage using pulsed wave radars, mean channel velocity from continuous wave Doppler radars, and their combined use to estimate discharge at sites that were collocated with conventional streamgauges. Potential stage biases caused by the thermal expansion and contraction of supporting structures due to diurnal temperature changes were examined. A dry concrete, flume showed the temperature-dependent stage variations were no more than 2 cm. Surface velocity retrievals needed to be adjusted to represent the mean channel velocity when estimating discharge. Different approaches were evaluated and application of two different, depth-dependent adjustment factors was found to yield the most accurate estimates. This study found that it is possible to get accurate discharge estimates from noncontact radar measurements, providing cost-effective solutions for remote sensing of ungauged streams. Lastly, radar measurements of the raw variables (i.e., stage and surface velocity) can be used in an early alerting context to detect flash floods in ungauged streams.

1. Introduction

Stream discharge estimates are of paramount importance for stormwater management, flood forecasting, estimating sediment load for water quality, water resources management, navigation, recreation, and endangered species protection and management. Conventional streamgauges, such as those operated and maintained by the U.S. Geological Survey (USGS), provide measurements of water depth (Eberts et al., 2018). To compute the discharge, an empirical relation is established between the stage, which is the measured water depth plus bed elevation, and discharge to compute a stage-discharge rating. These rating curves require manual, in-situ measurements of the variables to compute discharge (i.e., distribution of flow velocity, stream cross-section, stage) over a wide range of river flow conditions (Buchanan and Somers, 1969). Technicians collect these data approximately every six weeks using a combination of current meters and hydroacoustic devices. Instream and near-bank vegetation changes and sediment deposition and scour, which can become enhanced during floods, can change the shape of a previously surveyed cross-section and the associated rating curve (Mason and Weiger, 1995). Changes in the hydraulics and channel cross-section require regular visits and instream measurements. Remote sensing has increasingly become a more desired alternative to manual surveying and conventional, in-situ measurement techniques because remote-sensing instruments do not need to be in contact with the water (Moramarco et al., 2019). Remote-sensing instruments provide increased safety to the technicians and are less likely to be lost during major floods than fixed, traditional streamgauging equipment, in addition to providing the potential for less expensive operations and maintenance (Fulton et al., 2020).

Remote-sensing technologies used to estimate discharge in streams include cameras and radars. Image analysis using cameras, such as the large-scale particle image velocimetry (LSPIV) technique have

* Corresponding author.
E-mail address: jj.gourley@noaa.gov (J.J. Gourley).

https://doi.org/10.1016/j.jhydrol.2021.126809
Received 10 February 2021; Received in revised form 2 August 2021; Accepted 7 August 2021
Available online 13 August 2021

demonstrated the capability of estimating surface velocities in streams (Fujita et al., 1998; Creutin et al., 2003; Muste et al., 2008). Stringent procedures are followed to ensure usable image quality in long, wide natural channels, and operational applications are challenged by bandwidth requirements for transmitting video (Kim et al., 2007; Tauro et al., 2017). Detert (2021) provides a set of guidelines to help users improve their procedures for performing image-based surface velocity measurements. After its first introduction in 2000, various noncontact radar techniques have been utilized for stage and surface velocity measurements (Costa et al., 2000). Instruments include a helicopter-mounted radar, an X-band pulsed radar, coherent microwave systems, continuous wave microwave, monostatic UHF Doppler, and pulsed Doppler microwave radar (Lee et al., 2002; Melcher et al. 2002; Plant et al., 2005; Costa et al., 2006). These studies were primarily experimental and demonstrate the basic measurements of stage and surface velocity in rivers. Until now, very few research studies have assessed the uncertainty of noncontact measurements with radars (Welber et al., 2016; Fulton et al., 2020).

Our study is a component of the larger Automated NonContact Hydrologic Observations in Rivers project (ANCHOR; https://www.nssl.noaa.gov/projects/anchor/) that was originally motivated by the noncontact, radar-based discharge estimates presented in Costa et al. (2006). In the present study, we use a stream radar unit that integrates two noncontact radar methods to retrieve both the stage and surface water velocity of a stream simultaneously. Eight stream radars have been installed on bridges, culverts, and cables throughout the United States and provided year-round measurements with a typical temporal resolution of 5–10 min. The objectives of this study are as follows: (1) to identify and quantify the error in stage measurements by the nadir-pointing, pulsed wave radar, (2) to optimize the correction for translating surface water velocities from the Doppler radar to a mean channel velocity needed to compute discharge from noncontact measurements, and (3) to assess the sensors' capabilities to detect the rapid onset of flooding events in ungauged basins. Section 2 describes the physical settings of the radar deployments and the methods used for deriving discharge. Section 3 identifies sources of measurement uncertainty and quantifies them. Section 3 also reveals the characteristics of a major flash flooding event. Conclusions from the study and a discussion are summarized in Section 4.

2. Methods and materials

2.1. Study area

To represent a variety of meteorological, hydrologic, and hydraulic characteristics, eight stream radars have been installed on cables, culverts, and bridges across streams at locations in four states in the United States. As shown in Fig. 1, three are installed in Texas, two each in Arizona and Oklahoma, and one in Colorado. Site selection was based on several factors including proximity to a conventional streamgauge, a need for monitoring, cellular network signal strength, site security and access, and hydraulic suitability of the site for monitoring. These constraints permitted testing of the radars for a variety of hydrologic and hydraulic settings. The radars were installed on a bridge in an urban setting (Fig. 2a,b), above a small natural channel in a rural setting (Fig. 2c,d), on an instrumented flume in the desert (Fig. 2e,f), on a bridge above a river with frequent morphological changes (Fig. 2g,h), above a small creek upstream from a popular summer camp (Fig. 2i,j), on a box culvert over a spring-fed creek (Fig. 2k,l), above an engineered urban channel (Fig. 2m,n), and above a stream on a railway bridge (Fig. 2o,p). In general, it took two to three people a few hours to install the sensors. The basin areas for these streams range from 2 to 3676 km^2 and are characterized by different land-use settings including forested, urban, and desert (Table 1). The 5- or 10-minute logging rate is user-defined.

Cherry Creek is a tributary of the South Platte River that runs near Denver, Colorado (Fig. 2a). The area of the basin is 1059 km^2. According to the National Land Cover Database 2011 (NLCD 2011) (Homer et al., 2015), land use in the upper part of the basin is mostly vegetation (e.g., herbaceous and shrub/scrub), whereas the lower part is a developed area where the site is located. The relative proportions of sand, silt, and clay are 53.9%, 29.7%, and 16.4%, respectively as per CONUS soil datasets (Miller and White, 1998). The area has a mean basin slope of

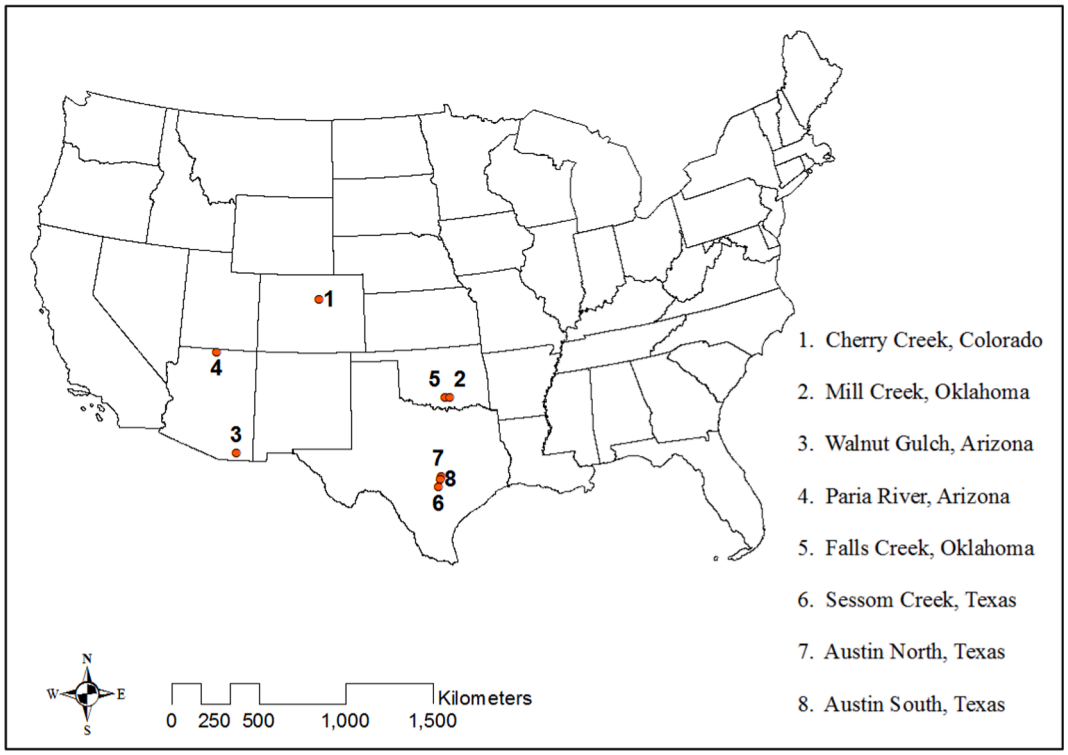

Fig. 1. Locations of the eight stream radars in four different states of the United States.

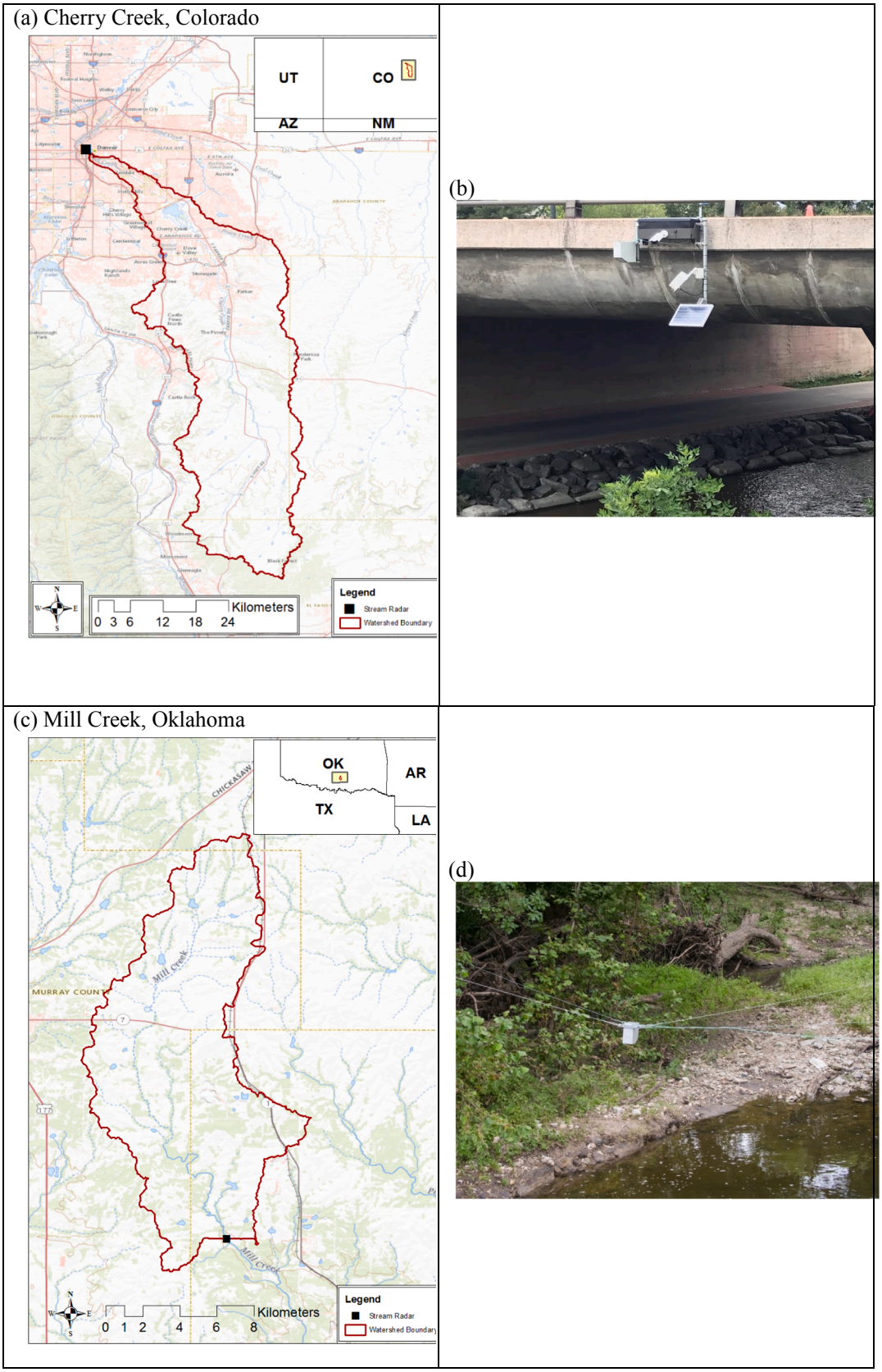

Fig. 2. Basin boundaries and site photographs for the eight sites shown in Fig. 1. Base map layers are provided by Environmental Systems Research Institute.

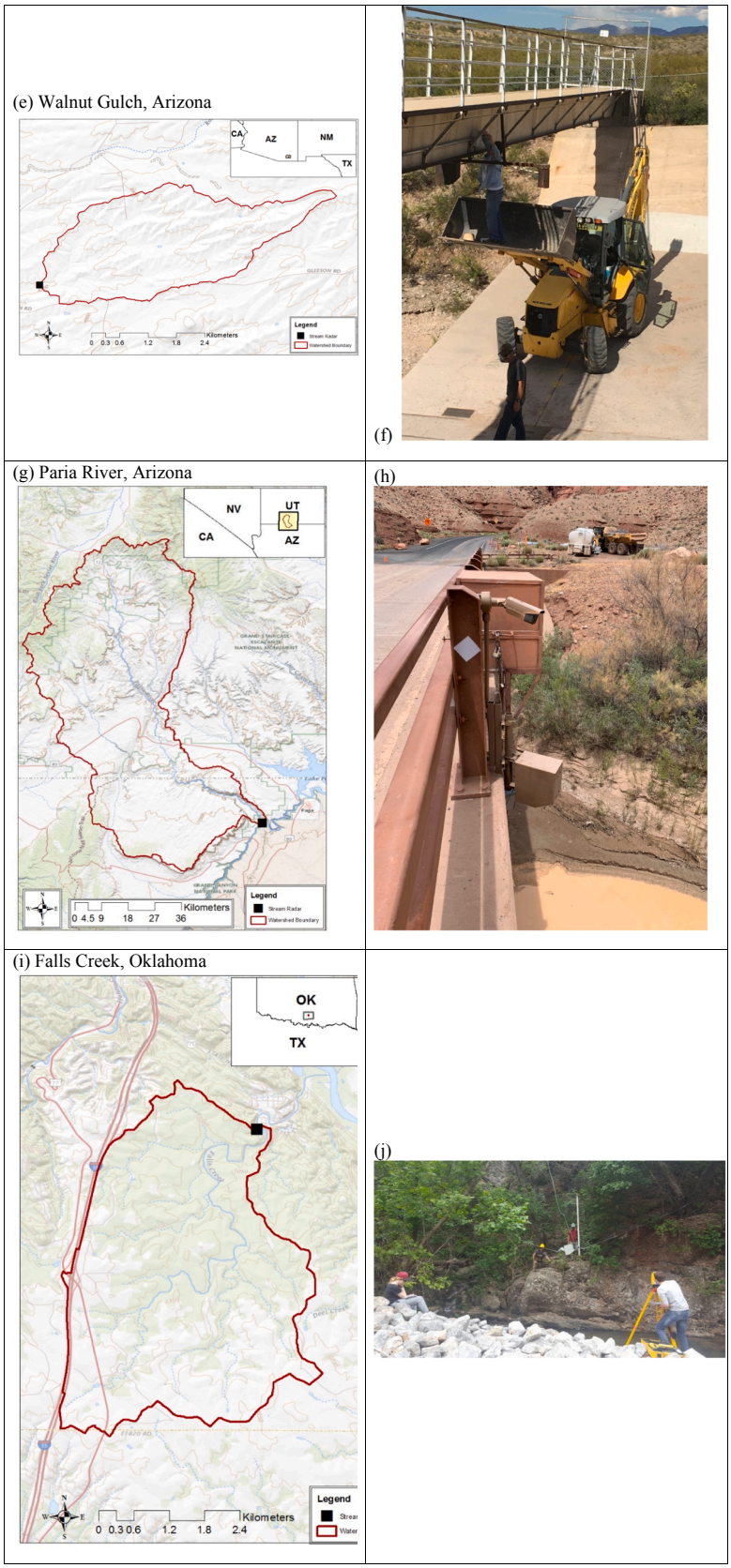

Fig. 2. (*continued*).

7.9%. The mean annual precipitation from 1981 to 2010 at the radar location is 404 mm (PRISM, 2004). The stream radar is mounted on a bridge here (Fig. 2b) and situated approximately 60 m upstream from a USGS streamgauge (ID – 06713500).

Mill Creek runs through rural Johnston County, Oklahoma. The basin area is 124 km^2 (Fig. 2c). The NLCD 2011 land use of the area is

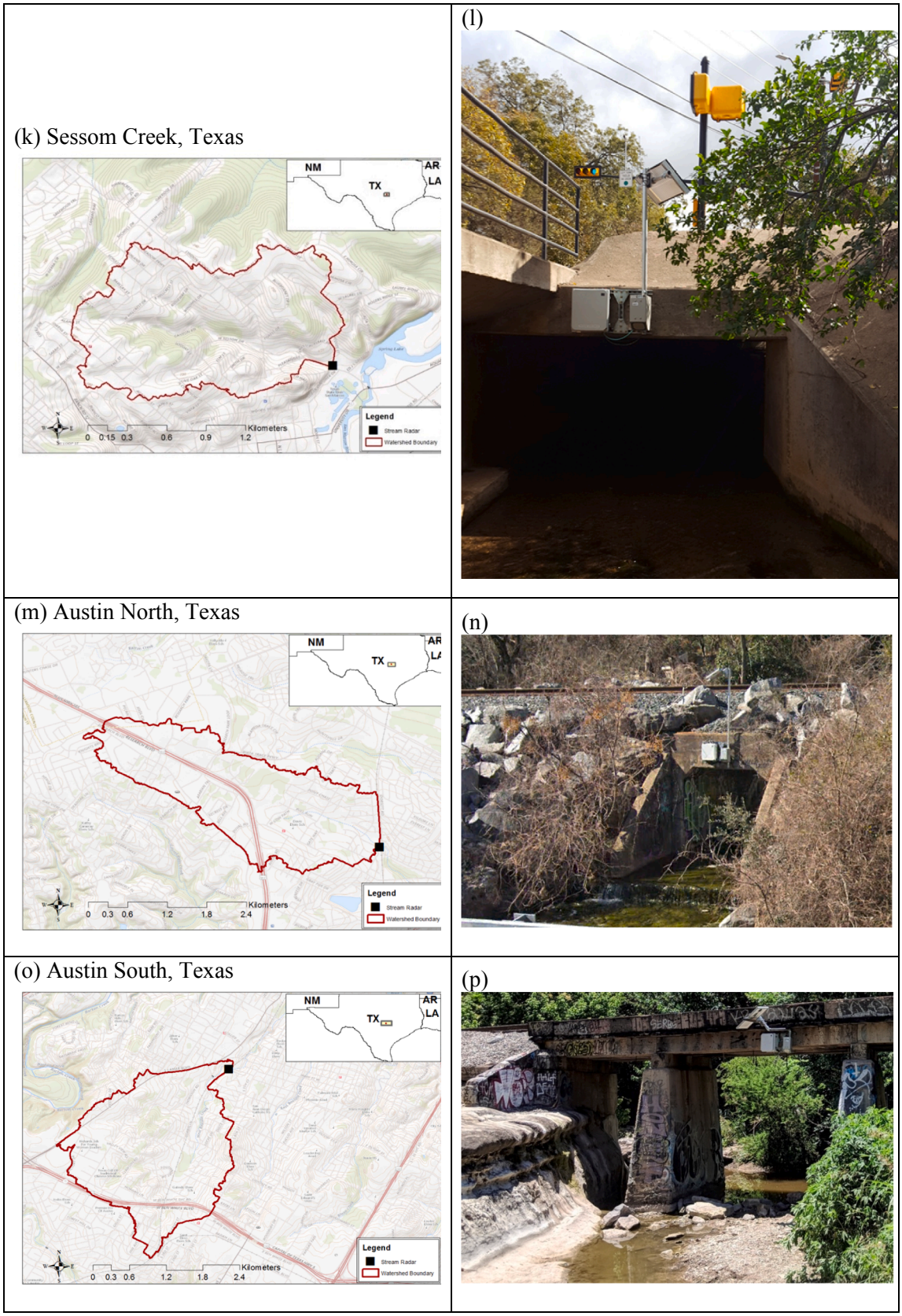

Fig. 2. (*continued*).

mostly herbaceous and hay/pasture lands. The soil texture has a relative proportion of sand, silt, and clay as 27%, 42.3%, and 30.7%, respectively. The area has a mean basin slope of 3.2% and the mean annual precipitation near the radar location is 1027 mm per year. The radar is cable mounted (Fig. 5) and has a USGS streamgauge approximately 30 m upstream from its position (ID – 07331200).

Table 1
Summary of basin characteristics and radar deployments for all the stations. (CL = collocated with a conventional streamgauge, NCL = Non-collocated with a conventional streamgauge).

Station	Basinarea (km^2)	Land Use	Radar Mounting	Status	Data Period		Temporal Data Resolution (minutes)
					Start	End	
Cherry Creek (39.7421, −104.9996)	1059	Urban	Bridge	CL	Aug 2017	Apr 2019	5
Mill Creek (34.4048, −96.8632)	124	Pasture/ Cropland	Cable	CL	Sep 2017	Sep 2018	10
Walnut Gulch (31.7417, −109.9947)	7.8	Desert	Bridge	CL	Jul 2018	Nov 2019	10
Paria River (36.8722, −111.5939)	3676	Desert	Bridge	NCL	Jul 2018	Oct 2019	10
Falls Creek (34.4222, −97.1130)	15.1	Forest	Cable	NCL	Mar 2017	Jun 2019	10
Sessom Creek (29.8906, −97.9367)	1.6	Urban	Culvert	NCL	Nov 2017	Jun 2019	10
Austin North (30.4160, −97.7300)	4.3	Urban	Culvert	NCL	Jul 2018	May 2019	5
Austin South (30.2480, −97.7670)	4.6	Urban	Bridge	NCL	Jul 2018	Sep 2018	5

The stream radar at Walnut Gulch is part of the dense instrumentation comprising the U.S. Department of Agriculture (USDA)/Agricultural Research Service's Walnut Gulch Experimental Watershed in southeast Arizona. Water moves through a concrete flume here and the size of the contributing area is 7.8 km^2 (Fig. 2e). The primary land-use type of the basin is desert vegetation (e.g., shrub and herbaceous). The relative proportions of sand, silt, and clay are 58%, 29.6%, and 12.4%, respectively. The basin has a moderately sloping mean gradient of about 12.1%. The mean annual precipitation amount is 356 mm. The radar is mounted on a bridge (Fig. 2f) and collocated with a conventional USDA streamgauge. Discharge data are provided only during events and can be just a few episodes per year during the monsoon.

Paria River is a tributary of the Colorado River that runs from southern Utah towards northern Arizona. It has a very large basin area of approximately 3676 km^2 for the radar location (Fig. 2g). The upper part of the basin has some vegetation land usages, but the rest of the area is mostly barren, desert land. For soil texture, the relative proportions of sand, silt, and clay are 56%, 23.3%, and 14.7%, respectively. The basin has a high mean slope of 20.9%. The area near the radar has a very low mean annual precipitation of 185 mm. The radar is mounted on a bridge (Fig. 2h) and has a USGS streamgauge (ID – 09382000) about 1.2 km upstream from its position. Because of this distance between the USGS streamgauge and the stream radar, it is not considered to be collocated to conduct direct discharge comparisons.

Falls Creek originates from the springs of the Arbuckle-Simpson aquifer and flows towards the northeast into the Washita River in Oklahoma. The size of the basin area for the stream radar location is 15.1 km^2 (Fig. 2i). The land uses mostly include grassland and different types of forest (e.g., evergreen and deciduous). The relative proportions of sand, silt, and clay are 23%, 63%, and 14%, respectively. The mean basin slope is 7% and mean annual precipitation is approximately 1000 mm. The radar is cable mounted (Fig. 2j) and not collocated with any other streamgauge.

Sessom Creek is a spring creek that drains to the San Marcos River in Texas. Water moves through a concrete box culvert. The contributing area at stream radar's location is only 1.6 km^2 (Fig. 2k). Land uses involve mostly development, open space, and evergreen forest. The soil texture has a relative proportion of sand, silt, and clay as 24.5%, 25.5%, and 50%, respectively. The mean basin slope is 11.6% and mean annual precipitation near the radar location is about 861 mm. The radar is mounted on a culvert as shown in Fig. 2l and there is no other streamgauge near the site location.

Austin North is sited on a tributary of Walnut Creek, which flows southeast into the Colorado River in Austin, Texas. The basin area for the stream radar location is 4.3 km^2 (Fig. 2m). The land uses of the area involve open space and moderate degrees of development. The relative proportions of sand, silt, and clay are 22.9%, 26.2%, and 51.0%, respectively. The mean basin slope is 5% and the mean annual precipitation is about 862 mm. The stream radar is mounted on a box culvert, which supports a train bridge (Fig. 2n), and it is not collocated with any other streamgauge.

The Austin South unit is placed above West Bouldin Creek, which flows northeast until it reaches the Colorado River in Austin, Texas. The radar location has a basin area of 4.6 km^2 (Fig. 2o). The area is a developed one that involves both open space and intense development. Soil texture has a relative proportion of sand, silt, and clay as 17.8%, 32.5%, and 49.8%, respectively. The basin has a mean slope of 7.7% and mean annual precipitation is 856 mm near the radar location. The radar is mounted on a train bridge (Fig. 2p) and there is no other streamgauge here.

2.2. Noncontact measurement principles

The stream radar units evaluated in this study are manufactured by SOMMER Messtechnik and alternatively known by their model name: RQ-30. The stage radar uses a pulsed 26 GHz microwave radar with a 10° beamwidth pointing in the nadir direction. The radar can operate from 0 to 15 m above the stream or 0–35 m, depending on the specific unit. Stream velocities are measured using a continuous wave 24 GHz Doppler radar with a 12° beamwidth and can look either in the upstream or downstream direction of the channel at a fixed 56° angle off nadir. The stage radar has a vertical resolution of 1 mm while the velocity radar has a resolution of 1 mm s^{-1}. The velocity sensor can operate in scenarios where the distance to the water surface is 0.5–35 m. Both units are powered by a single 12 V 15 amp-hr battery that is charged using a 30 W solar panel. Data are typically logged every 5–10 min and transmitted hourly using cellular data communications. The HyQuest Solutions' IP datalogger iRIS 350FX datalogger has an alerting feature that automatically increases the frequency of data logging and transmitting to 1 min when thresholds are and can send SMS text messages.

2.2.1. Water level measurement

For water level measurement, the radar sensor transmits a short microwave pulsed signal to the stream and receives its echo as the pulse reflects off the water surface. The time lag between sending and receiving the signal is directly proportional to the distance between the sensor and water surface and is determined as below:

$$h = \frac{ct}{2} \tag{1}$$

where h is the distance between the water surface to the sensor (m), c is the speed of light (m s^{-1}), and t is the measured time (s) of the two-way travel distance of the pulse. The distance (E) between the bottom of the sensor and a ground reference level corresponding to the mean of the channel bottom elevation (GZ) is measured when the unit is installed (Fig. 3).

Bridges, culverts, and cables experience thermal expansion and contraction throughout the day as they heat and cool in response to atmospheric diurnal temperature changes. These thermal expansions/contractions may cause the radar to move from its original position leading to a deviation from the actual stage measurements. To evaluate this effect, stage data are selected during periods with steady base flow, and two such periods are chosen to confirm the consistency of the behavior throughout the whole timeseries. For each station, air

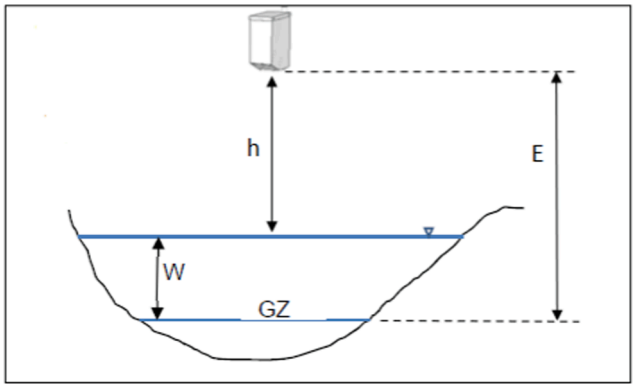

Fig. 3. Water level measurement technique by stream radar (modified from Sommer, 2014). To retrieve water depth (W), the distance (E) between the sensor and a reference level corresponding to the mean of the channel bottom elevation (GZ) is entered into the sensor so that the sensor can automatically determine W from the difference between E and the measured h.

Table 2
Summary of air temperature data used in the study.

Station	Airport Name	Data Resolution (minutes)	Data Period	
			Start	End
Cherry Creek	Denver Centennial Airport, Colorado	60	Jul 2018	Aug 2019
Mill Creek	Ardmore Municipal Airport, Oklahoma	60	Mar 2017	Jun 2019
Walnut Gulch	Douglas Bisbee International Airport, Arizona	60	Aug 2017	Jul 2019
Paria River	Page Municipal Airport, Arizona	60	Jul 2018	Jul 2019
Falls Creek	Ardmore Municipal Airport, Oklahoma	60	Mar 2017	Jun 2019
Sessom Creek	San Marcos Municipal Airport, Texas	60	Nov 2017	Jun 2019
Austin North	Austin Bergstrom International Airport, Texas	60	Jun 2018	May 2019
Austin South	Austin Bergstrom International Airport, Texas	60	Jun 2018	May 2019

temperature data are collected from the "Local Climatological Data (LCD)" database of National Oceanic and Atmospheric Administration (NOAA) (NOAA, 2019), which typically records temperature at airports (Table 2). It is assumed in this study that air temperature measured at the closest airport is representative of the temperature experienced at the stream radar location, while more accurate measurements could be made at the site or obtained from a nearby personal weather station. The distances from the stream radar to the nearest surface weather station varied from 6.8 km to as far as 73.5 km. Finally, stage and air temperature data are evaluated for each steady base-flow period.

2.2.2. *Surface velocity measurement*

The surface velocity measurement is based on the principle of surface scattering and the Doppler shift. The radar sensor transmits a signal to the stream at fixed angle of 56° off nadir. This signal is backscattered by the movement of the small-surface waves that occur on the water surface and are assumed to be propagating in various directions but all riding on the large-scale motion on the water. Various means have been demonstrated to retrieve water surface velocity from surface scattering and Doppler shift (Plant et al., 2005; Fulton et al., 2020). Here, we present the physical basis for retrieving the surface velocity, while the Sommer manufacturer applies their own spectral analysis to the signal and retrieval algorithm.

The lengths of these short waves are determined by the Bragg resonance condition (Plant et al., 2005) as:

$$\lambda_b = \frac{\lambda}{2sin\theta} \tag{2}$$

where, λ_b is the wavelength of the resonant water wave (i.e., the Bragg wave) (m), λ is the wavelength of the radar beam (m), and θ is incidence angle (degree). When we use the values associated to the K-band radar (i.e., $\lambda = 1.25$ cm, $\theta = 56$), we find a wavelength associated to the small-surface wave scatterers on the water surface of 0.75 cm.

When the transmitted signal returns to the sensor, there is a motion-induced frequency shift due to the Doppler effect. By calculating the shift in frequency, the surface velocity is computed as follows (Fulton and Ostrowski, 2008):

$$v = f_d \lambda_b \tag{3}$$

where, v is the surface velocity (m/s), f_d is the radar-measured Doppler shift in frequency (Hz or s^{-1}), and λ_b is the wavelength of the resonant water wave (m).

The radar sensor measures surface velocities of the illuminated footprint via a 12° beamwidth. This area increases with the distance between the water surface and the sensor. From the velocity distribution of the illuminated area, the Doppler spectrum is created, analyzed, and used by the algorithm to report the velocity. The sensor can detect movement both towards and away from the sensor, and the shift in frequency depends on this direction. For better detection, the water body requires observable disturbances at the surface. Minimum disturbances can also be produced by wind or rain (Costa et al., 2006). Wind drift can bias surface velocity measurements depending on site characteristics such as in a narrow valley, a stream with low hydraulic gradient, and with surface velocities less than 0.15 m/s (Fulton et al., 2020). In the Fulton et al. (2020) study, they use an anemometer collocated with a stream radar and then propose a wind drift correction scheme. The correction scheme is based on the Prandtl von Karman wind velocity distribution; the component of the wind vector component that is in the direction of the stream and the stream radar's orientation is then added or subtracted to arrive at the wind-corrected surface velocity value.

High wind speeds can also potentially affect measurements from the cableway-mounted systems by altering their verticality. The computation of velocity in the RQ-30 takes into account the inclination of the sensor, as measured by an onboard inclinometer. For fixed mounts, this inclination measurement is performed once (first measurement after a reboot or config file change). For cableway-mounted radars, a new inclination measurement is applied with each velocity measurement. This mostly accounts for gradual movement of the mounting points (as cables and supporting structures expand/contract and branches grow). Cables are installed with high tension to avoid high-frequency swing, but in the case of high winds causing inclination changes on the order of the measurement time, this will be reflected as a low value in the "quality" parameter that is logged for every velocity measurement. The quality parameter is based on the Doppler spectrum and reflects the sharpness of the peak velocity and the signal-to-noise ratio. Negative quality values indicate poor quality velocity measurements and these data are rejected when comparing to collocated station data.

2.3. *Discharge computation*

From the conservation of mass theory, volumetric discharge is computed as below:

$$Q = \bar{v}A \tag{4}$$

where, Q is the discharge (m^3/s), $\bar{v}$is the mean channel velocity (m/s), and A is the wetted cross-sectional area (m^2).

The vertical velocity distribution in natural, open-channel flows is

characterized by a velocity dip below the free surface and can be modeled by a modified log-wake law (Guo and Julien, 2008). Quick changes of velocity are mainly observed near the channel bottom and banks. It is generally assumed that the depth-mean velocity of a channel can be found at 0.6 times the depth below the water surface for relatively shallow channels, or from the mean of the velocities found at 0.2 and 0.8 times the depth below the surface for deep channels. For example, if a channel has a total water depth of 10 m, then the depth-mean velocity can be estimated at a depth of 6 m below the surface, or, from the mean of the velocities at depths of 2 and 8 m below the surface. Mean channel velocity for a natural channel can be estimated from the surface velocity by multiplying it by a constant (Rantz, 1982). Therefore, discharge from radar observations at any time step i is computed as below:

$$Q_i = k_g v_i A_i \tag{5}$$

where, Q_i is the discharge (m^3/s), k_g is a "global" k coefficient that relates the surface velocity to mean channel velocity, v_i is the surface velocity (m/s), and A_i is the wetted cross-sectional area (m^2).

2.3.1. Determination of k value

A "k" coefficient of 0.85 to 0.90 is used to translate a surface velocity to a mean-vertical velocity (Rantz, 1982). This assumes the vertical velocity profile can be approximated using a logarithmic distribution or power law; however, if the vertical velocity distribution is non-standard - where the maximum velocity occurs at depth - a different coefficient is required for each vertical in the channel cross-section. Although multiple studies accept the validity of the default value for natural channels, from recent experiments it is found that the actual value of k depends on the roughness of the bed material, the place where the measurement is made, and Reynolds number (Costa et al., 2000; Melcher et al., 2002; Costa et al., 2006; Le Coz et al., 2012; Welber et al., 2016). Also, secondary currents, presence of vegetation, or tidal fluctuations can affect k (Johnson & Cowen, 2017). Considering different criteria, numerous k values have been recommended such as 0.85 and 0.93 for base-flow and high-flow conditions, respectively (Harpold et al., 2006); 0.79 to 0.93 depending on the roughness condition of the channel bed (Polatel, 2006); 0.75 to 0.83 for high-flow situations in mountain channels (Jodeau et al., 2008); 0.79 to 1.72 in compound or irregular channels (Sun et al., 2010); 0.72 to 0.79 for channel bed consisting of gravel (Dramais et al., 2011); 0.86 to 1.18 due to secondary currents (Gunawan et al., 2012); 0.82 to 0.93 for varying Reynolds number (Johnson & Cowen, 2016); and so on.

A cross-section averaged k coefficient, or global k coefficient (i.e., k_g in Equation (5)), is needed to compute discharge if there is only a single surface velocity measurement available along a given stream cross-section. This is the case with the fixed deployment of the stream radars. Given the larger roughness values and shallower depths near the banks, global k coefficients are expected to be lower than the local k coefficients reported above. Welber et al. (2016) examined the differences between global and local k coefficients and found that the variability of the global values is considerably smaller than the local values. Moreover, they found that the global k coefficients obtained in smoother channels fall into the range of the local k coefficients of 0.80–0.91 with a mean of 0.86.

An alternative but related approach to relate surface velocities measured by the stream radar to mean channel velocities is based on the entropy or probability concept using the ϕ parameter (Chiu and Chiou, 1986; Chiu, 1987; Chiu, 1989). This concept is based on an assumed velocity distribution and is adaptable to cross-sections where the maximum velocities are found either at the surface or below the surface. Fulton et al. (2020) directly validated the ϕ parameters used to convert radar-measured velocities to mean velocities using conventional, in-situ measurements. They found values for the ϕ parameter ranging from 0.52 to 0.78, which yielded very close agreement to mean velocities from conventional, mechanical current meters or hydroacoustics. Moreover, ϕ does not vary with stage, velocity, discharge, bed form, or approach angle, which makes ϕ valuable when dealing with temporal changes in physically based models (Fulton et al., 2020).

To optimize the k values for all three collocated stations, the following multi-objective function is developed. The intention is to develop a function that considers the entire time series as well as event-based statistics relevant for flooding. The developed objective function is:

$$\Psi = \frac{1}{3}NSE + \frac{1}{3}\left(1 - \frac{VE}{100}\right) + \frac{1}{3}\left(1 - \frac{PE}{100}\right) \tag{6}$$

where, Ψ is a dimensionless quantity that is expected to vary between 0 and 1, *NSE* is the Nash-Sutcliffe Efficiency for whole time series, *VE* is the mean volumetric error of an event (%), and *PE* is the mean error in peak-value of an event (%). The multi-objective function is designed to equally weight errors in event-based peak flow, volume, and the *NSE* describing the agreement for the entire time series.

NSE is a metric used frequently in hydrology to describe how well two time series covary and is well suited objective function for this type of analysis (Servat and Dezetter, 1991; Legates and McCabe, 1999). Use of *NSE* is also recommended by ASCE (1993) and chosen to represent the overall accuracy level of the measurements in this study. The event-based metrics of mean volumetric error (*VE*) and peak-flow error (*PE*) and are computed as below:

$$VE = \frac{1}{n}\sum_{i=1}^{n} abs\left(\frac{(V_{P,i} - V_{O,i})}{V_{O,i}}\right) \tag{7}$$

where $V_{P,i}$ is the volume of the i^{th} event integrated under the hydrograph of radar-estimated discharge (m^3), $V_{O,i}$ is the volume of the i^{th} event integrated under the hydrograph of conventional discharge (m^3), n is the total number of events, and *abs* operator indicates the absolute value of the variables within the bracket.

$$PE = \frac{1}{n}\sum_{i=1}^{n} abs\left(\frac{(P_{P,i} - P_{O,i})}{P_{O,i}}\right) \tag{8}$$

where $P_{P,i}$ is the peak-flow value of the i^{th} event of radar-estimated discharge (m^3/s), and $P_{O,i}$ is the peak-flow value of the i^{th} event of conventional discharge (m^3/s).

For each collocated station, this study computes the multi-objective function using both single-k and double-k values. For all the trials with k values, a code is developed in python and the methods below are considered during computation. We note that the guidance for default values generally apply to local k coefficients, and we apply these findings to represent global k values with the understanding that there can be differences due to the influences of bed roughness, radar illumination area, and water depth.

- The previous studies show local k values can vary roughly from 0.7 to 1.0, even greater than 1.0, based on the channel and flow conditions. However, for single-k optimization, this study varies the k value from 0.7 to 1.0 with a trial increment of 0.001.
- The double-k optimization is based on the work of Hauet et al. (2018). With this method, a threshold of water depth limit is set first and then two different k values are assigned for the depths above and below the threshold. For Cherry Creek and Mill Creek, this threshold is varied from 1.8 to 2.1 m as they are natural channels. Under each threshold of depth, the lower k value (for depths lower than the threshold) is varied from 0.75 to 0.85, while higher the higher k value (for depths higher than the threshold) is varied from 0.9 to 1.0. The increments for depth threshold and k value are 0.003 m and 0.001, respectively.
- Because Walnut Gulch uses a concrete, supercritical flume, this k value is varied from 0.85 to 1.0 with an increment of 0.001 following the work of Hauet et al. (2018).

2.3.2. Calculation of wetted cross-sectional area

Discharge estimates using the stage-velocity radar data assume that there is a stable cross-section. Changes to the bathymetry can have a negative effect on the discharge estimates. Therefore, at first, surveys are conducted to find a stable channel bottom for each site and then the cross-sections are established at the selected location of the channel. A cross-section of any channel is measured using a conventional total station surveying method. The vertical elevations along the line where the radar makes stage measurements are recorded by a total station survey relative to the reference level (e.g., point of zero flow, corresponding to the channel bottom or lower to allow for scour). However, in the case of Mill Creek, the elevation of the floodplain at its left bank is complemented from a 1-m resolution digital elevation model (DEM) (USGS, 2020) and then merged with the surveyed datapoints to complete the cross section.

Cross-section data (e.g., station and elevation with respect to North American Vertical Datum of 1988) of a channel are further loaded into an online calculator (NWS, 2020) that gives the corresponding wetted area for any water depth. For each site, wetted areas corresponding to a range of water depths are determined, where the range varies from the minimum recorded stage value for that station to the maximum one with an increment of 0.03–0.06 m. Finally, an equation is developed from the best fit of these data points and for any i^{th} stage value, A_i is derived from the equation. For Cherry Creek, a stage-area rating curve is provided by the USGS. It is noted that stage-area and stage-discharge ratings would be affected by changes to the channel bathymetry caused by sediment deposition or scour, vegetation growth, etc. The site selection for the stream radars considered the stability of the channel bottom. In cases where the channel bathymetry may be evolving, a stage-velocity rating curve using the stream radar variables would need to be developed and monitored. A sudden shift in the stage-velocity relation could be indicative of change in the channel's cross-section, which would bias the calculation of the discharge. Alternatively, the channel bathymetry can be regularly surveyed or even retrieved using remote-sensing approaches such as a bank-to-bank scanning light detection and ranging (lidar) as proposed in Gourley (2017). With this measurement, the wetted cross-sectional area (and thus discharge) will be more accurate than inferred under the assumption of a static cross-section.

3. Results and discussions

3.1. Uncertainty in stage measurements

Fig. 4 shows the time series of radar-measured stage and temperature for two of the bridge-mounted radars (Cherry Creek, Walnut Gulch), a cable-mounted radar (Mill Creek), and a radar mounted on a concrete box culvert (Austin North). The bridge- and cable-mounted radars generally exhibit positive correlations with air temperature (Fig. 4a–c), while the culvert at Austin South has a weaker, negative correlation (Fig. 4d). It is believed that with an increase in temperature, expansion of the bridge materials causes the bridge deck and cables to slightly sag, which results in the radar deflecting downward from its original position yielding an apparent higher stage. This would cause the distance between the radar and the water surface (h in Fig. 3) to decrease resulting in an overestimation of stage. The opposite would occur when the air temperature cools and the bridge materials contract. In the case of Falls Creek, it was discovered that a collocated water treatment plant regularly pumps water from the creek that potentially affects the steady state of base-flow conditions and the positive correlation with temperature was not observed. The radar at Austin South is mounted on a wooden train bridge that produces vibration due to frequent trains crossing of the bridge. As a result, the stage records become noisy for this station at irregular intervals and correlation of stage with temperature cannot be readily observed.

To further quantify the correlation between stage and temperature, the correlation coefficient (r) between these two variables is computed

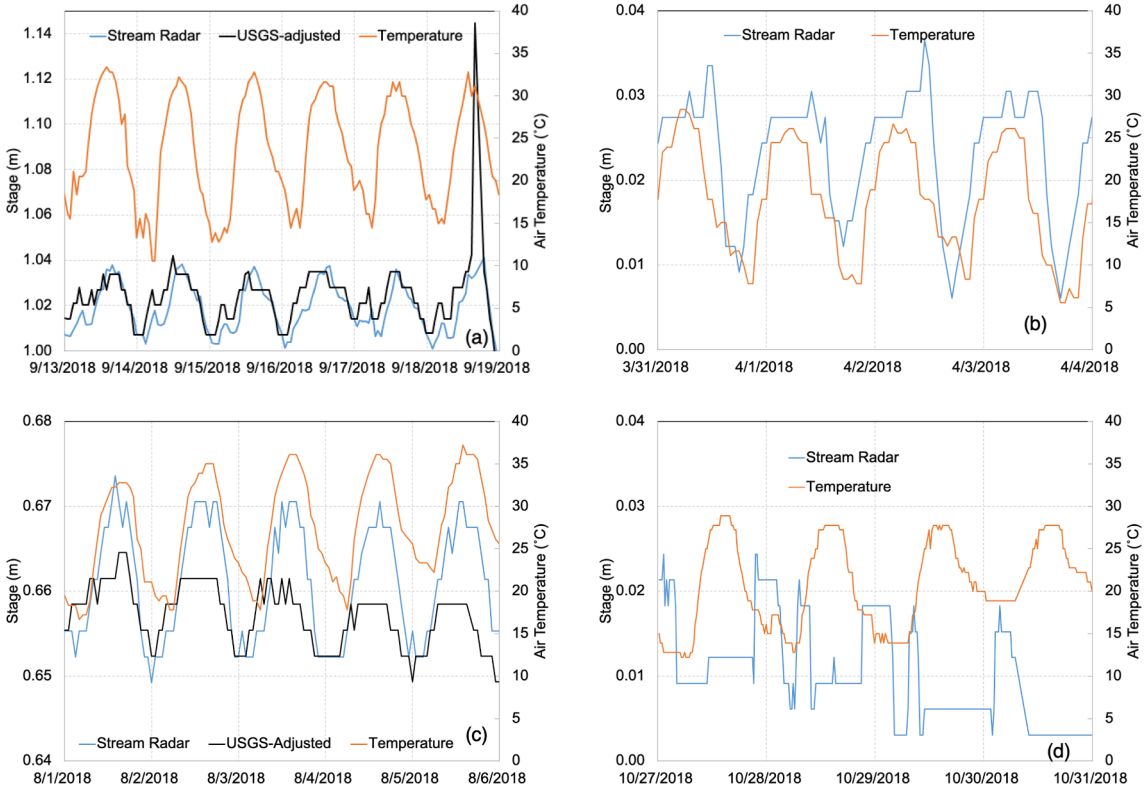

Fig. 4. Time series of radar-measured stage (m) and atmospheric temperature (℃) during stable base-flow periods for (a) the bridge-mounted radar at Cherry Creek, (b) the bridge-mounted radar at Walnut Gulch site, (c) the cable-mounted radar at Mill Creek, and (d) the culvert-mounted radar at Austin North. Adjusted stages from collocated USGS stage measurements are shown in (a) and (c).

Table 3
Correlation coefficient (r) between stage and temperature for the selected data periods.

Station	Data Period 1		r	Data Period 2		r
	Start	End		Start	End	
Cherry Creek	Sep 9 2018	Sep 18 2018	0.563	Apr 7 2019	Apr 10 2019	0.729
Mill Creek	Sep 9 2017	Sep 13 2017	0.772	Jul 31 2018	Aug 8 2018	0.526
Walnut Gulch	Mar 30 2018	Apr 10 2018	0.742	Jan 10 2019	Jan 18 2019	0.639
Paria River	Jul 20 2018	Jul 30 2018	0.779	Jul 17 2019	Jul 26 2019	0.804
Falls Creek	Jul 22 2017	Aug 2 2017	0.155	Jun 9 2019	Jun 18 2019	−0.139
Sessom Creek	Oct 12 2017	Dec 6 2017	−0.258	May 5 2018	May 21 2018	−0.441
Austin North	Oct 23 2018	Nov 2 2018	−0.475	Jan 2 2019	Jan 12 2019	−0.129
Austin South	Aug 15 2018	Aug 23 2018	0.330	Aug 27 2018	Sep 5 2018	0.023

(Table 3). For Cherry Creek, Mill Creek, Walnut Gulch, and Paria River, r varies between 0.526 and 0.804, which indicates a moderate, positive correlation between stage and air temperature. Although Falls Creek has a cable-mounted radar, the r values during the two base-flow periods are 0.155 and −0.139, indicating no correlation. As previously mentioned, this is due to the effect on base-flow conditions caused by the pumping from the water treatment plant. As for the two box culverts at Sessom Creek and Austin North, they both show weaker, negative correlations. The stage records at Austin South have little correlation with air temperature ($r = 0.023$ and 0.330) during stable base-flow conditions due to the added vibration of the bridge.

The analysis conducted herein was to assess potential effects of the mounting structures on the stage data measured by the radars. Given that Walnut Gulch is a normally dry wash, we analyze the stage and temperature data during time periods for which there was zero observed flow. This analysis provides an indication of the temperature dependence of the stage data in the absence of any water in the stream. The diurnal temperature range results in an apparent stage change of approximately 2 cm, owing to the thermal expansion of concrete of the supporting bridge over the concrete flume.

Stage data from the collocated USGS stations at Cherry Creek and Mill Creek are provided for base-flow periods. The stages at these sites could potentially be affected by temperature-dependent changes in the supporting structures and water in the underlying streams. The USGS stations at Mill Creek and Cherry Creek use conventional gas-purge (bubbler) systems. Note that their time series are independent from the radar measurements or structures used for mounting them. Curiously, the two conventional gauges also show a diurnal temperature dependence of the stage. The USGS data indicate a daily variation in the observed stage as high as 3 cm at Cherry Creek (Fig. 4a) and approximately 1 cm at Mill Creek (Fig. 4c). The stream radar diurnal variations in stage are the same as the USGS observations at Cherry Creek and approximately 2 cm at Mill Creek, or 1 cm greater than the USGS observations.

It is plausible that these observed stage changes are due to urban and rural outdoor water uses, respectively, during the summer months. The coefficients of volume expansion for steel and concrete are similar to one another at 35×10^{-6}–C^{-1}. On the other hand, the coefficient of volume expansion for water is 210×10^{-6} C^{-1}, or approximately six times greater than the expansion potential of the supporting materials. It is difficult to quantify the uncertainty in the stream radar stage measurements when there is water in the channel. Nevertheless, from the comparisons provided in this analysis, including those from a dry concrete flume at Walnut Gulch, we can estimate the diurnal variation caused by the thermal expansion of the supporting structures to be within 2 cm.

3.2. Uncertainty with k value

3.2.1. Discharge comparison with default, global k value (0.85)

Prior to estimating discharge, radar-retrieved velocities can be compared to in situ measurements using conventional current meters or hydroacoustics at multiple depths along the stream cross-section. The reader is referred to the Fulton et al. (2020) study that conducted velocity validations using the same type of stream radars as used in this study. In our case, k_g values are initially applied using a default value and later optimized using the conventional discharge measurements as a constraint. For the three stream radars that are collocated with conventional streamgauges, discharge is estimated by reducing the measured surface velocity using a default k_g factor of 0.85. We note that this value has been suggested as a default for local k values and not necessarily a global k value; nevertheless, it provides a starting point for estimating discharge. This value is then multiplied by the wetted cross-sectional area, which is computed from the stage measurements combined with the stream's cross-section as described in Section 2.3. Table 4 provides the statistical results when comparing to discharge from the conventional streamgauges for the entire time series listed in Table 1.

Table 4 shows that the radar observations of all the collocated stations are quite accurate in providing the discharge estimates when compared to their respective streamgauge data. The sample sizes vary owing to different hydroclimatologies, sensor reporting frequencies, and length of period over which the sensor was operational. The USGS data at Mill Creek, Oklahoma, were considered provisional for a three-month period in the spring of 2018 but were later approved following this study's analysis period. Further, many low flow cases were not considered in the analysis due to poor quality velocity measurements from the stream radar. The sample size at Walnut Gulch is even smaller due to the episodic nature of flows in the dry wash during the monsoon. In all cases, the radar sensors yield NSE and r values close to 1.0, and the NB values are generally small with a slight high bias at the Cherry Creek site. The data are also presented in the form of scatterplots in Fig. 5. These results are representative of the sensors' capability of estimating discharge without any parameter tuning on streams with a measured or known, stable cross-section.

One objective of the ANCHOR project is to assess the sensors' capabilities of detecting rapid-onset flooding in vulnerable areas to provide early alerting to local authorities. Fig. 6 compares times series of discharge from the stream radars to the conventional gauges for several high-flow events. While the statistical comparisons for the entire time series indicate very close agreement with the conventional gauges, we can identify the following discrepancies in the event-based comparisons: (1) underestimation in peak-flow values, (2) underestimation in the total water volume integrated throughout the high flow event, and (3) high-frequency fluctuations in the stream radar discharge values. Regarding the event-based underestimation of both peak flows and volume, one potential reason could be an improper setting of the ground reference level (GZ), which is meant to be the mean of the channel bottom elevation, as illustrated in Fig. 3. This setting would result in bias that would affect the entire time series at both high and low flows. The event-based hydrographs in Fig. 6 indicate, however, that the discharge estimates generally agree at the beginning and end of the events, yet the

Table 4
Statistical scores of discharge comparison for the collocated stations (n = number of datapoints; NSE = Nash-Sutcliffe Coefficient, unitless; r = Coefficient Correlation, unitless; NB = Normalized Bias; RMSE = Root Mean Square Error).

Station	n	NSE	r	NB (%)	RMSE (m^3/s)
Cherry Creek	150,552	0.925	0.972	13.56	0.27
Mill Creek	654	0.931	0.967	4.78	1.27
Walnut Gulch	64	0.976	0.996	−2.28	1.33

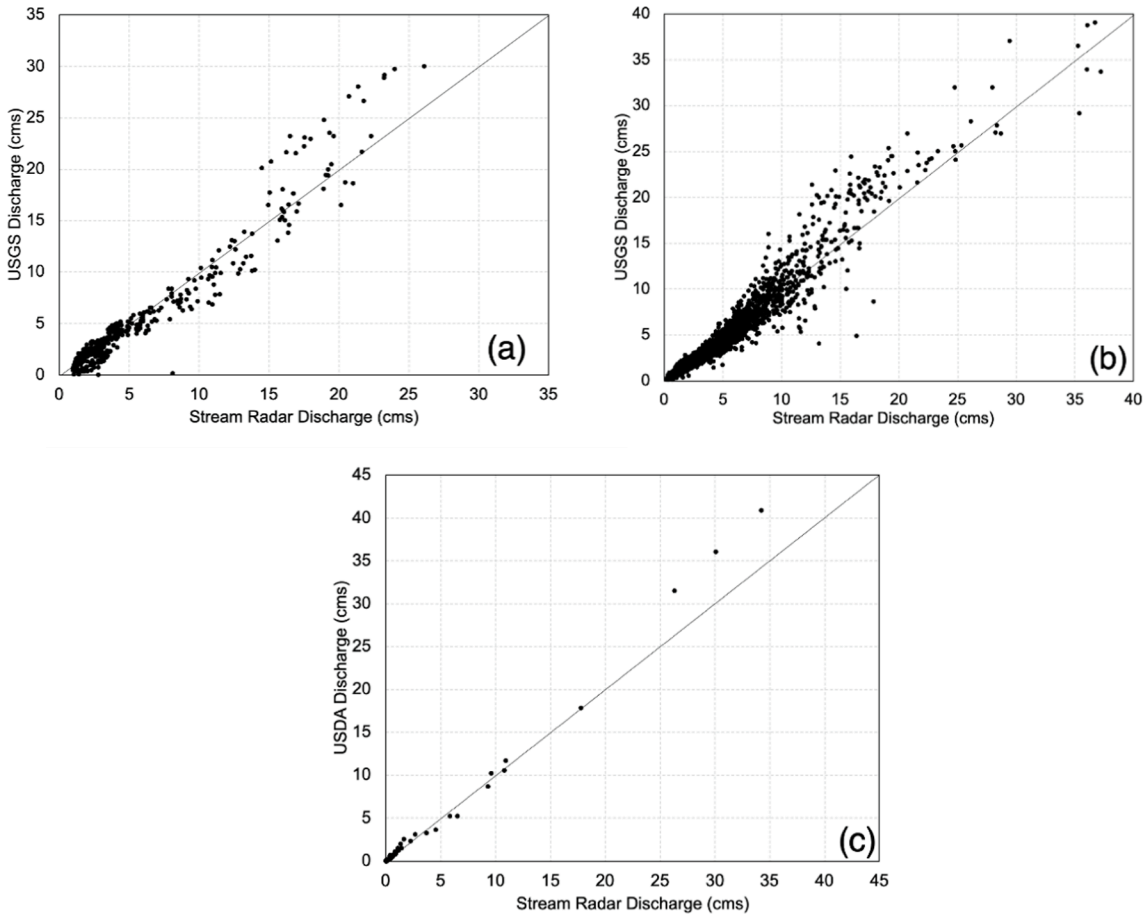

Fig. 5. Scatter plots of discharge (in $m^3 s^{-1}$, or cms) as measured by a conventional station and the stream radars at (a) Mill Creek, (b) Cherry Creek, and (c) Walnut Gulch using a default k_g coefficient of 0.85.

peak flows are still underestimated by the stream radar. This stage-dependent bias is evaluated in more detail in the next section.

Conventional gauges represent the event dynamics from stage measurements that are then converted to discharge using a rating curve. In the case of the stream radars, the time-varying velocity and stage data are both used to compute discharge. The fluctuations in the stream radar hydrographs are found to be caused by the velocity measurements and not the stage. The noise in the surface velocity retrievals can be caused by small waves initiated by wind and/or rain, secondary currents, and potentially some slight swinging of the instrument for the cable-mounted radars. Nevertheless, these fluctuations are deemed random errors and are assumed to not cause bias. These random errors can be mitigated by using a smoothing window on the velocity (or discharge) data.

3.2.2. *Sensitivity analysis for global k value*

The prior analyses indicate that while the stream radars yield discharge values with default k_g values that agree quite well with conventional gauges (e.g., NSE close to 1), there are non-negligible peak-flow and volumetric errors during flood events. More specifically, the radar-driven discharge estimates are accurate during low flows but underestimate during high flow events. Prior studies (i.e., Harpold et al., 2006; Hauet et al., 2018) have recommended the use of two k values to represent base-flow and high-flow conditions. Lower k values are recommended for base flows when the roughness of the stream bed has more effect on the surface velocities. At high flows, the roughness from the bed materials is less influential on the surface water velocities. So, in the following, we explore the optimization of two k values for each site, applied in a global sense. The approach adopted herein is to simultaneously quantify the event-based hydrograph errors and also consider the accuracy of the discharge estimates for the entire time series.

Table 5 shows the global k values that maximize the multi-objective function for each collocated station. For all the stations, the results are improved due to double k_g-value optimization. For single-k_g optimization, k_g varies between 0.78 and 0.91 while for double-k_g, it varies between 0.75 and 0.96. In general, the highest Ψ values are obtained for double-k_g optimization, although the relative differences between the results for two different k_g values are very small. Fig. 7 shows scatter plots of the radar-estimated and measured discharge from the collocated stations, similar to Fig. 5. The radar-estimated discharges in Fig. 5 are using the global k values of 0.85, while Fig. 7 shows the values for the optimized single- and double-k_g values. The values yielded from the double-k_g scheme are closer to the diagonal for all three stations. This applies to both high and low flows.

For Cherry Creek, the optimized single k_g value (0.78) is found to be less than the default one and it reduced the VE and PE error by almost 4% with an increase in the NSE score. For double-k_g optimization, the threshold depth limit differs by only 0.12 m from the recommended value (2 m) by Hauet et al. (2018). For the k_g values, the higher one (0.89) is very close to their recommended value of 0.9, whereas the lower one (0.75) slightly deviates from the recommended value of 0.8. The VE error is almost halved and PE is also reduced by 4%. Because the total number of events is 26 for Cherry Creek, this is a substantial improvement in hydrograph errors and therefore, these k_g values can represent the whole timeseries well.

As for Mill Creek, the single k_g value (0.83) is slightly lower than the default 0.85, and the NSE, VE, and PE scores do not change that much

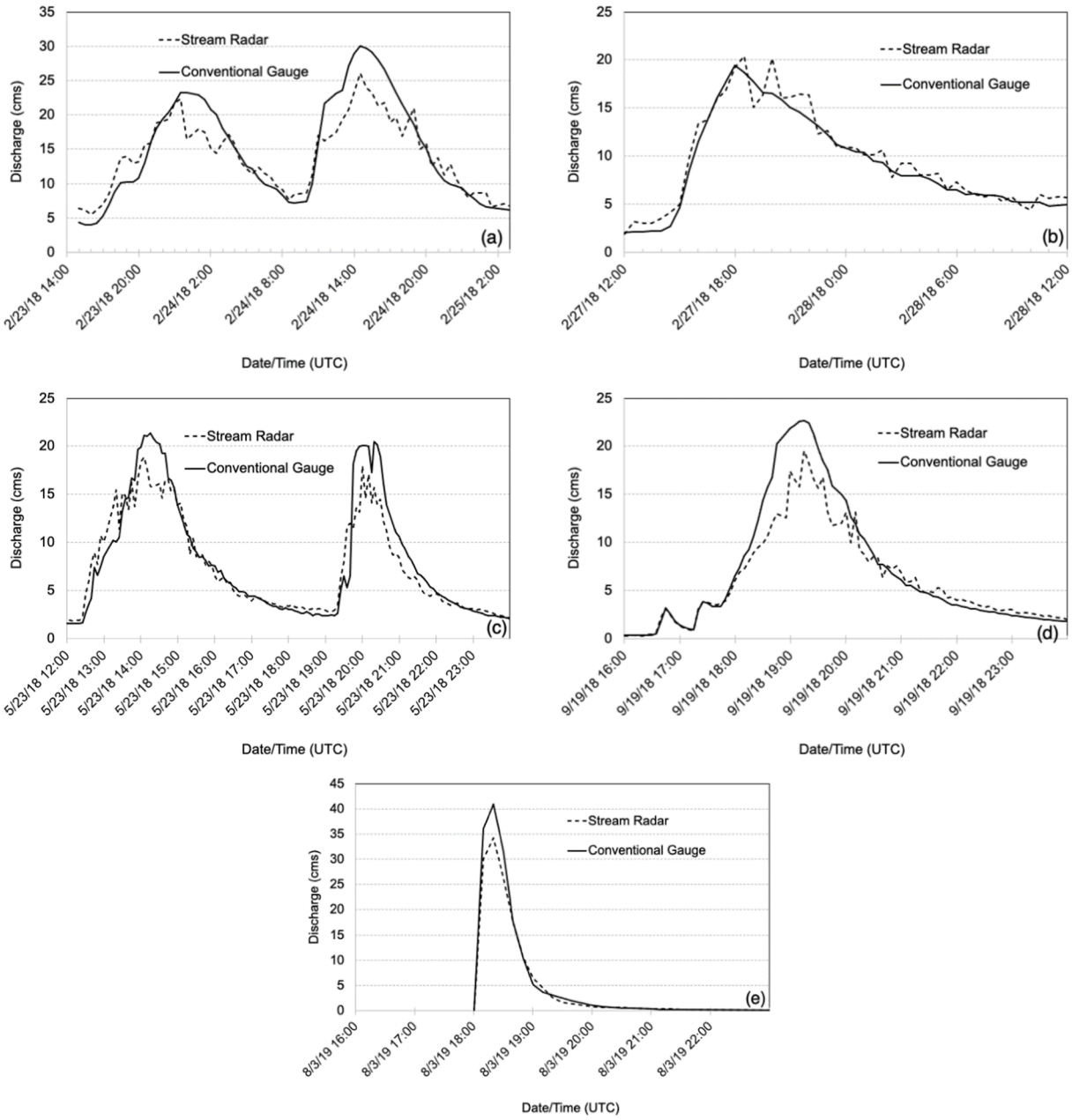

Fig. 6. Hydrographs of radar-measured and conventional discharge estimates (in $m^3 s^{-1}$, or cms) for flooding events at (a, b) Mill Creek, (c, d) Cherry Creek, and (e) Walnut Gulch using a default k_g coefficient of 0.85.

from the results found with the default. However, the double k_g value provides higher NSE score as well as lower VE and PE scores. The threshold of depth limit (1.9 m) is only slightly lower than the recommended 2.0 m threshold. The lower k_g value is very close to 0.8, while the higher k_g value is 0.96.

For Walnut Gulch, the optimized, single-k_g value (0.91) is similar to the recommended value (0.9) by Hauet et al. (2018). However, the event-based errors do not change that much from the default k_g-derived errors. For double-k_g optimization, the k_g value is quite similar (0.85) to the default one when the depth is less than 0.9 m, and for greater depths the optimized k_g value is found to be 1.0. With the use of these two k_g values, VE becomes less than 1%, PE is almost halved and NSE approaches 1.0 (0.979). With the increase of water level, channel bed roughness in a concrete flume is expected to have less effect on mean channel velocity and therefore, a k_g value close to 1.0 for depths above 0.9 m is physically realistic.

The prospects for using the sensors to quantify discharge on previously ungauged basins is promising. Our results indicate that the use of a single, default k_g value of 0.85 will yield NSE values greater than 0.9 indicating very low error covariance. There is some modest benefit with the optimization approach in reducing the event-based peak-flow and total volume errors, which requires in situ measurements not unlike the need to establish a rating curve in conventional gauging. However, the next section explores the use of the stage and velocity measurements with no in situ measurements required a priori.

3.3. Early detection of flooding events

One objective of the stream radar units is to assess the capability of detecting rapid-onset flooding events in ungauged basins where there are vulnerable assets downstream. One such setting is the Falls Creek stream radar placed upstream from a camp near Davis, Oklahoma

Table 5
Results on multi-objective function optimization for the three stream radars that are collocated with conventional gauges. The best value for each metric is in boldface.

Station	Number of events	k_g value	Ψ	NSE	VE (%)	PE (%)
Cherry Creek	26	0.85 (default)	0.883	0.925	13.22	14.29
		0.78	0.912	0.939	9.57	10.88
		0.89 for stage > 1.9 m and 0.75 for stage ≤ 1.9 *m*	**0.923**	**0.949**	**7.56**	**10.43**
Mill Creek	4	0.85 (default)	0.872	0.931	10.80	20.73
		0.83	0.878	0.929	9.25	20.20
		0.96 for stage > 1.9 m and 0.81 for stage ≤ 1.9 *m*	**0.901**	**0.958**	**8.15**	**17.17**
Walnut Gulch	4	0.85 (default)	0.943	0.976	5.78	9.04
		0.91	0.954	0.989	6.20	6.58
		1.00 for stage >0.9 m and 0.85 for stage ≤ 0.9 *m*	**0.979**	**0.998**	**0.70**	**5.40**

(Gourley, 2017). The camp hosts as many as 7500 children, teenagers, and staff at a given time during the summer months. On 18 June 2015, the region was struck by heavy rainfall (up to 800 mm) from a re-intensifying Tropical Storm Bill. In the camp, a bus was submerged and some campers were isolated for more than a day. In coordination with the camp director, the unit was installed on the stream upstream from the camp in March 2017 with the intention to provide early alerting. The datalogger nominally logs data every 10 min and transmits them every hour. The datalogger was initially programmed with subjective alert thresholds for stage exceeding 1.22 m or velocity exceeding 1.22 m s^{-1}. When the stage or velocity exceeds the alert threshold, data are logged and transmitted every 5 min. Note that this frequency can be increased to data logging and transmission every 1 min when in alarm status. On 19–20 May 2017, severe weather affected the region resulting in a tornado warning issued by the local National Weather Service forecast office and heavy rainfall rates over the basin. The time series plot of radar-measured surface velocity and stage in Fig. 8 indicates the velocity exceeded the alert threshold at 0300 UTC and the stage exceeded its threshold at 0315 UTC. The rate of the river stage increase was 2.57 m hr^{-1}. Interestingly, the velocity first exceeded the alert threshold and preceded the associated rise in stage by approximately 30 min. This offset in the rising limbs of the velocity and stage hydrographs is attributed to a celerity effect caused by inertial accelerations and/or a pressure gradient from a non-negligible slope in the water surface. In fact, the stage-discharge hysteresis is discussed in detail in Muste et al.

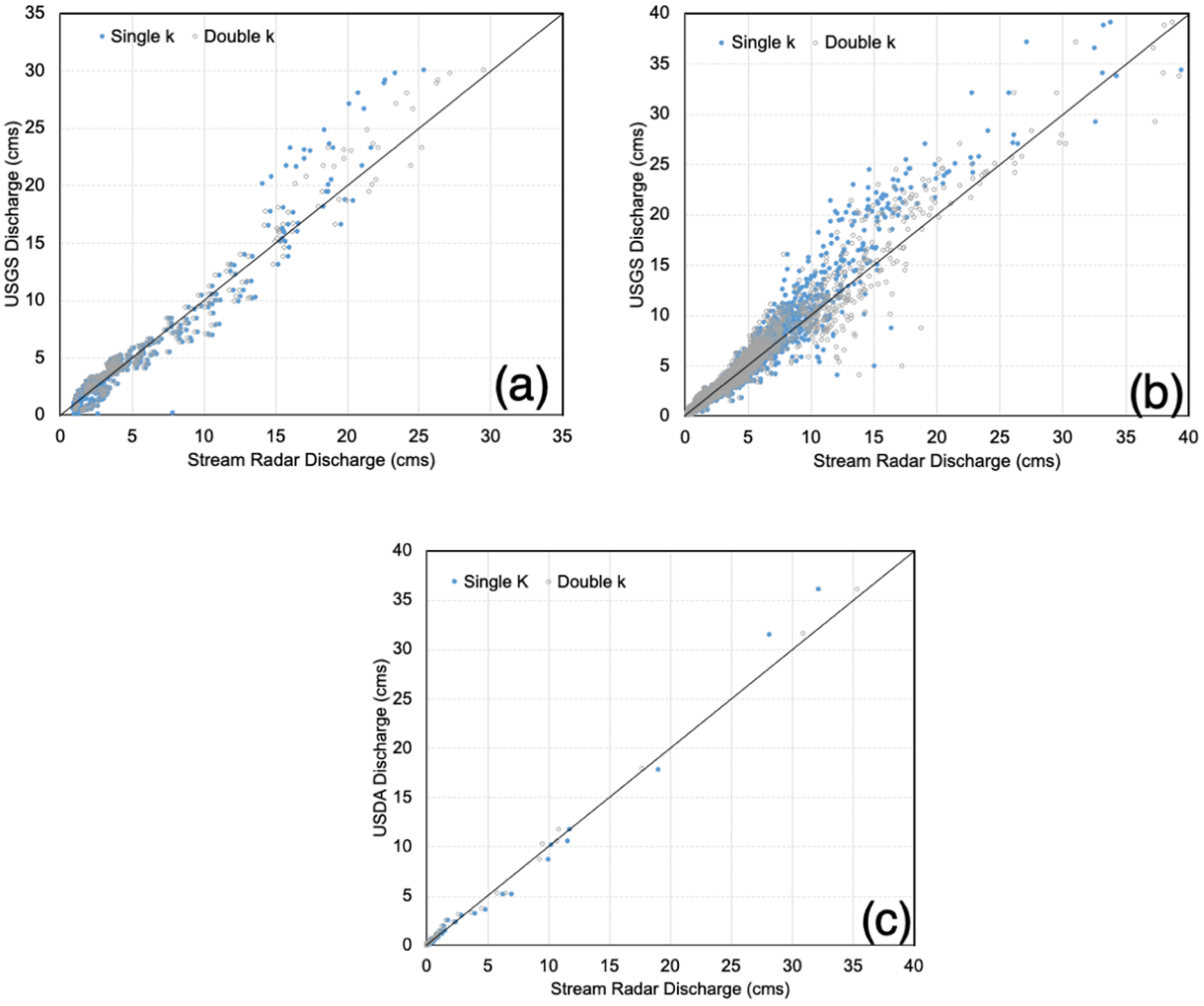

Fig. 7. Scatter plots of discharge (in m^3 s^{-1}, or cms) as measured by a conventional station and the stream radars using the single- and double-k_g optimization schemes at (a) Mill Creek, (b) Cherry Creek, and (c) Walnut Gulch.

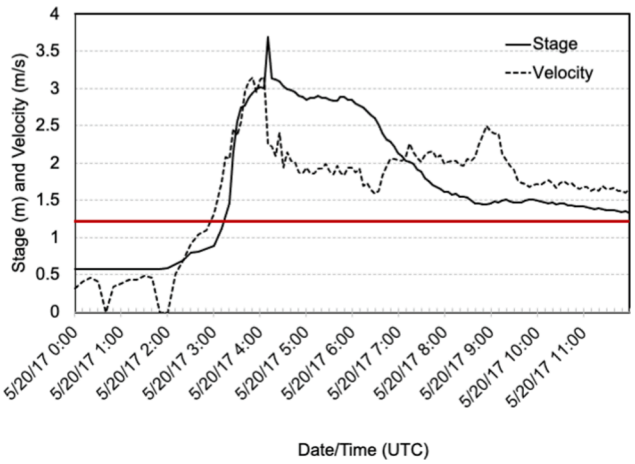

Fig. 8. Hydrographs of radar-measured stage (solid) and surface velocity (dashed) for a flash flooding event at the Falls Creek site near Davis, Oklahoma. The initial alert thresholds for both stage and velocity that was used for this event is shown in red. (For interpretation of the references to colour in this figure legend, the reader is referred to the web version of this article.)

(2020). Unsteady flow conditions arise when the stage varies rapidly during events that cause substantial slopes in the water surface relative to the channel bed slope. Situations of extreme rainfall falling on relatively flat terrain can yield the hysteretic behavior. From analytical considerations, Muste et al. (2020) also show that a direct manifestation of unsteady flows is phase sequencing between the time series of velocity, discharge, and stage, in that order. This phase sequencing has rarely been reported in field measurements (Rowinski et al., 2000). Given the early arrival of the velocity wave, the stream radar combined with the alerting features of the data logger enabled more timely identification of an impending, rapid-onset flooding event downstream.

Following the event, the project team visited the radar to survey high-water marks and assess the condition of the stream radar (Fig. 2j). The stream had risen to the height of the bottom of the unit itself. Upon inspection, it was discovered that despite the damage that was incurred to the radars' housing, the waterproofing of the individual radars in the unit succeeded so that they continued to operate throughout and after the event. Nevertheless, debris flowing down the stream impinged upon the supporting cables causing great tension on the housing and resulted in the damage shown in Fig. 9. The mounting was subsequently fortified to prevent stress on the housing in the future, and the unit was raised from its original position. Furthermore, the datalogger was programmed

Fig. 9. Photographs of the Falls Creek, Oklahoma, stream radar following the 17 May 2017 flash flooding event.

to alert on the following thresholds: 0.91 m, 0.91 m s^{-1}, 1.52 m, 1.52 m s^{-1}, 2.13 m, 2.13 m s^{-1}. If any of these thresholds are exceeded, then the data logging and transmitting frequency is increased to 5 min and SMS alerts are sent to local stakeholders. This event demonstrated that a stream radar unit could be used as an indicator of flash flooding at an ungauged, vulnerable location without the need for cross-section surveys, in situ measurements for developing the rating curve, or even establishment of bankfull flooding thresholds. Moreover, the real-time capabilities of data delivery and SMS alerting enabled the measurements of surface velocity and stage to be useful without the need for estimating discharge. In fact, it could be argued that these variables lend themselves to be more understandable and thus useful to stakeholders.

4. Discussion and Conclusions

To evaluate the effectiveness of remote-sensing technologies in noncontact measurement of stream variables (water level and surface velocity), eight stream radars have been installed at high-priority locations across the United States. The radars are mounted on bridges, culverts, and cables and have provided measurements for at least 1 year with a temporal resolution of 5–10 min. The eight streams represent a variety of hydrologic, hydraulic, and hydroclimatological characteristics, and three of them are collocated with conventional streamgauges. This study is part of the Automated NonContact Hydrologic Observations in Rivers (ANCHOR) project and aims to identify and characterize errors in the raw measurements, to optimize correction factors so the data can be used to estimate discharge, and to assess whether the real-time transmission of alerts based on stage and surface velocity measurements can be useful in an early alerting context.

Potential biases were assessed on stage measurement due to diurnal temperature changes causing expansion and contraction of the supporting bridges, cables, and culverts. For bridge- and cable-mounted systems, these stage measurements would be biased in direct correlation with temperature. In the cases of bridges and cables, the sensor could sag closer to the water surface giving the impression of an increase in stage. The opposite could occur with the culvert-mounted units. We compared stage data from the stream radars to observations from collocated, conventional bubbler streamgauges at Cherry Creek, Colorado, and Mill Creek, Oklahoma. These independent USGS streamgauges also showed a diurnal fluctuation in stage, which is attributable to outdoor water uses during the summer months. The stream radar had the same fluctuations as the USGS observations at Cherry Creek and had about 1 cm more variation than the USGS stage measurements at Mill Creek. It is difficult to quantify the uncertainty in stream radar stage measurements caused by thermal expansion of the supporting structures when water is present in the channel. The coefficient of volume expansion with water is approximately six times larger than with either steel or concrete. And, as we saw in our analyses, outdoor water uses can result in actual diurnal fluctuations in stage. Without a detailed analysis of the thermal properties of the culverts, bridges, and cableways, it is difficult to definitively quantify the effect of thermal expansion on stage at all sites. However, stage variations were assessed at Walnut Gulch, Arizona, when the concrete flume was completely dry. The maximum temperature-induced stage change was found to be 2 cm at this site, and the other collocated sites showed that the stage variations were not greater than this amount. Lastly, when estimating discharge, surface velocity retrievals during low-flow periods must consider ambient wind velocities as they can become biased.

Discharge comparisons at the collocated stations show that the use of a k_g value of 0.85 to convert surface velocities to represent a mean, channel velocity yield NSE values greater than 0.9. During substantial flooding events, peak-flow values are underestimated. The concept of using double-k_g values, which is normally applied to convert surface velocities to depth-averaged velocities for different stages and hydraulic conditions by Hauet et al. (2018), is a valid approach to get accurate results across the spectrum of flows including low flows and floods. With

the optimized k_g values, the statistical metrics indicate that the radar-based discharge estimates can be as accurate as in situ, conventional streamgauges, and have acceptable event-based hydrograph errors (less than 10% volumetric and peak-value error) during floods. Nevertheless, the k_g-value optimization requires a collocated, conventional streamgauge, which comes with the costs of regular visits to establish the stage-discharge rating curve. Our results at three sites reveal that the use of a single, default k value of 0.85 to be considered as a global k value yield NSE values greater than 0.9, indicating the degree of accuracy that can be obtained without the requirement of in situ measurements of velocity profiles.

The use of the single, default k value, nominally reported to convert surface velocities to depth-averaged values, applied here to represent the mean channel velocity may be a bit fortuitous for the three collocated sites. One would expect lower global k values to represent mean channel velocity compared to the local k values reported in the literature. In the case of Walnut Gulch, Arizona, the concrete flume represents a very smooth channel so that the local k value can approximate the mean across the cross-section, which agrees with results reported in Welber et al. (2016). In the case of Cherry Creek, Colorado, the unit was situated on a bridge approximately 6 m above the water surface. Given the 12° beamwidth of the Doppler radar and 56° off-nadir pointing angle, the radar illuminates more than 50% of the stream's width. This means that the inferred global k includes a representative distribution of surface velocities across the stream, and thus can approximate the local k values reported in the literature. In the case of Mill Creek, Oklahoma, the radar was situated at a location in the channel during base-flow conditions where the largest surface velocities were expected (see Fig. 2d). However, the channel is not as straight as desired at this location, and it is plausible that the radar measures surface velocities that are not the maxima along the cross-section; this results in the retrieved velocity to approximate a mean surface velocity rather than the maximum. Considerations of the radar siting that include the area illuminated in the stream affect the quality of the discharge estimates.

In this study, five out of the eight ANCHOR stream radars are situated over ungauged streams. These serve different purposes including low-flow monitoring of a spring-fed creek for sustaining endangered species on Sessom Creek, Texas, monitoring high flows that affect bridges carrying trains (Austin South and Austin North, Texas), and detecting flash floods above vulnerable camping areas (Falls Creek, Oklahoma). In the latter case, it was demonstrated that the sensors are capable of detecting surface velocities and river stages that pose hazards to life and property. There was a notable phase sequencing between the surface velocity and stage, indicative of unsteady flows caused by a large slope in the water surface relative to the mild channel bed slope. It turns out this observation would be valuable in an early alerting context. Alert thresholds based on stage and velocity values can be subjectively determined for a given site, input to the datalogger, and then used to increase the data logging and transmitting frequency and to alert local authorities and stakeholders by sending them SMS text messages. Further, the early alerting capabilities do not necessarily require detailed cross-section surveys or optimized k values to estimate discharges; the measurements of stage and surface velocity are sufficient.

Based on experience gained throughout the ANCHOR project, we provide some insights that can maximize data quality and quantity. Siting an instrument is key to its success. The channel would need to have uniform, relatively straight flow at the chosen site and a stable cross-section. Further, a site would need to have adequate cellular network coverage for transmitting the data. There are instances in which radio transmitters are being used to send the signal up to a ridge location where there is better cellular data coverage. The batteries are charged with a solar panel, so having good visibility toward the equator improves the power budgeting. Optimal siting of the units also needs to consider the degree of public access to reduce the instances of vandalism. In closing, this study provides experiences gained at diverse locations and will hopefully motivate future studies and efforts to promote additional sensing of earth's freshwater resources.

CRediT authorship contribution statement

Mushfiqur Rahman Khan: Formal analysis, Writing – original draft. **Jonathan J. Gourley:** Conceptualization, Supervision, Writing – review & editing. **Jorge A. Duarte:** Data curation, Software. **Humberto Vergara:** Project administration. **Daniel Wasielewski:** Funding acquisition, Investigation, Resources. **Pierre-Alain Ayral:** Investigation, Resources. **John W. Fulton:** Conceptualization, Resources.

Declaration of Competing Interest

The authors declare that they have no known competing financial interests or personal relationships that could have appeared to influence the work reported in this paper.

Acknowledgements

Funding was provided by NOAA/Office of Oceanic and Atmospheric Research under NOAA-University of Oklahoma Cooperative Agreement #NA16OAR4320115 and #NA16OAR4590234, U.S. Department of Commerce. Any use of trade, firm, or product names is for descriptive purposes only and does not imply endorsement by the U.S. Government. The authors declare no conflicts of interest, and the funders had no role in the design of the study; in the collection, analyses, or interpretation of data; in the writing of the manuscript, or in the decision to publish the results. The manuscript was greatly improved following the constructive comments from three independent reviewers and internal reviews supplied by the USGS.

Data availability

The air temperature data used in this study were obtained from the NOAA/National Center for Environmental Information at the following location: https://www.ncdc.noaa.gov/data-access/land-based-station-data/land-based-datasets/quality-controlled-local-climatological-data-qclcd. All USGS data used for validation can be obtained online (https://doi.org/10.5066/F7P55KJN). The time series data for all eight stations analyzed in this study (and their specific locations) have been placed in the public domain (doi:10.5281/zenodo.4526127).

References

ASCE (American Society of Civil Engineers), 1993. Criteria for evaluation of watershed models. Journal of Irrigation and Drainage Engineering, 119(3), 429-442.

Buchanan, T. J. & Somers W. P., 1969. Discharge measurements at gaging stations. Techniques of Water Resources Investigations. Available online: https://doi.org/10.3133/twri03A8 (accessed on 12 January 2021).

Chiu, C.-L., Chiou, J.-D., 1986. Structure of 3-D Flow in rectangular open channels. J. Hydraul. Eng. 112 (11), 1050–1067.

Chiu, C.-L., 1987. Entropy and probability concepts in hydraulics. J. Hydraul. Eng. 113 (5), 583–599.

Chiu, C.-L., 1989. Velocity distribution in open channel flow. J. Hydraul. Eng. 115 (5), 576–594.

Costa, J.E., Cheng, R.T., Haeni, F.P., Melcher, N., Spicer, K.R., Hayes, E., Plant, W., Hayes, K., Teague, C., Barrick, D., 2006. Use of radars to monitor stream discharge by noncontact methods. Water Resour. Res. 42 (7) https://doi.org/10.1029/2005WR004430.

Costa, J.E., Spicer, K.R., Cheng, R.T., Haeni, F.P., Melcher, N.B., Thurman, E.M., Plant, W.J., Keller, W.C., 2000. Measuring stream discharge by non-contact methods: A proof-of-concept experiment. Geophys. Res. Lett. 27 (4), 553–556.

Creutin, J.D., Muste, M., Bradley, A.A., Kim, S.C., Kruger, A., 2003. River gauging using PIV techniques: a proof of concept experiment on the Iowa River. J. Hydrol. 277 (3-4), 182–194.

M. Detert How to avoid and correct biased riverine surface image velocimetry Water Resources Research 57 2021 e2020WR027833 10.1029/2020WR027833.

Dramais, G., Le Coz, J., Camenen, B., Hauet, A., 2011. Advantages of a mobile LSPIV method for measuring flood discharges and improving stage–discharge curves. J. Hydro-environ. Res. 5 (4), 301–312.

Eberts, S., Woodside, M., Landers, M., & Wagner, C., 2018. Monitoring the pulse of our Nation's rivers and streams—The U.S. Geological Survey streamgaging network: U.S.

Geological Survey Fact Sheet 2018–3081. Available online: https://doi.org/10.3133/fs20183081 (accessed on 12 January 2021).
Fujita, I., Muste, M., Kruger, A., 1998. Large-scale particle image velocimetry for flow analysis in hydraulic engineering applications. J. Hydraul. Res. 36 (3), 397–414.
Fulton, J.W., Mason, C.A., Eggleston, J.R., Nicotra, M.J., Chiu, C.L., Henneberg, M.F., Laveau, C.D., 2020. Near-field remote sensing of surface velocity and river discharge using radars and the probability concept at 10 U.S. Geological Survey streamgages. Remote Sens. 12 (8), 1296.
Fulton, J., Ostrowski, J., 2008. Measuring real-time streamflow using emerging technologies: Radar, hydroacoustics, and the probability concept. J. Hydrol. 357 (1-2), 1–10.
Gourley, J.J., 2017. In pursuit of flash flood data. Eos 98. https://doi.org/10.1029/2018EO079723.
Gunawan, B., Sun, X., Sterling, M., Shiono, K., Tsubaki, R., Rameshwaran, P., Knight, D. W., Chandler, J.H., Tang, X., Fujita, I., 2012. The application of LS-PIV to a small irregular river for inbank and overbank flows. Flow Meas. Instrum. 24, 1–12.
Guo, J., Julien, P.Y., 2008. Application of the modified log-wake law in open-channels. J. Appl. Fluid Mech. 1, 17–23.
Harpold, A.A., Mostaghimi, S., Vlachos, P.P., Brannan, K., Dillaha, T., 2006. Stream discharge measurement using a large-scale particle image velocimetry (LSPIV) prototype. Trans. ASABE 49 (6), 1791–1805.
Hauet, A., Morlot, T., Daubagnan, L., Paquier, A., Rivière, N., 2018. Velocity profile and depth-averaged to surface velocity in natural streams: A review over a large sample of rivers. E3SWC 40, 06015. https://doi.org/10.1051/e3sconf/20184006015.
Homer, C., Dewitz, J., Yang, L., Jin, S., Danielson, P., Xian, G., Coulston, J., Herold, N., Wickham, J., Megown, K., 2015. Completion of the 2011 National Land Cover Database for the conterminous United States–representing a decade of land cover change information. Photogramm. Eng. Remote Sens. 81 (5), 345–354.
Jodeau, M., Hauet, A., Paquier, A., Le Coz, J., Dramais, G., 2008. Application and evaluation of LS-PIV technique for the monitoring of river surface velocities in high flow conditions. Flow Meas. Instrum. 19 (2), 117–127.
Johnson, E.D., Cowen, E.A., 2016. Remote monitoring of volumetric discharge employing bathymetry determined from surface turbulence metrics. Water Resour. Res. 52 (3), 2178–2193.
Johnson, E.D., Cowen, E.A., 2017. Remote determination of the velocity index and mean streamwise velocity profiles. Water Resour. Res. 53 (9), 7521–7535.
Kim, Y., Muste, M., Hauet, A., Bradley, A., Weber, L., Koh, D., 2007. Uncertainty analysis for LSPIV in-situ velocity measurements. In: Proceedings of the Congress-International Association of Hydraulic Engineering and Research, p. 81.
Le Coz, J., Pobanz, K., Faure, J.-B, Pierrefeu, G., Blanquart, Bertrand & Choquette, Y. (2012). Stage-discharge hysteresis evidenced by multi-ADCP measurements. River Flow 2012 - Proceedings of the International Conference on Fluvial Hydraulics. 2. 1277-1283.
Lee, M.-C., Lai, C.-J., Leu, J.-M., Plant, W.J., Keller, W.C., Hayes, K., 2002. Non-contact flood discharge measurements using an X-band pulse radar (I) theory. Flow Meas. Instrum. 13 (5-6), 265–270.
Legates, D.R., McCabe, G.J., 1999. Evaluating the use of "goodness-of-fit" measures in hydrologic and hydroclimatic model validation. Water Resour. Res. 35 (1), 233–241.
Mason, R.R., Weiger, B.A., 1995. Steam gaging and flood forecasting, A partnership of the U.S. Geological Survey and the National Weather Service. U.S Geol. Surv. Fact Sheet FS-209-95, 1–4.
Melcher, N.B., Costa, J.E., Haeni, F.P., Cheng, R.T., Thurman, E.M., Buursink, M., Spicer, K.R., Hayes, E., Plant, W.J., Keller, W.C., Hayes, K., 2002. River discharge measurements by using helicopter-mounted radar. Geophys. Res. Lett. 29 (22), 41-1–41-4.
Miller, D.A., White, R.A., 1998. A Conterminous United States Multilayer Soil Characteristics Dataset for Regional Climate and Hydrology Modeling. Earth Interact 2 (2), 1–26. https://doi.org/10.1175/1087-3562(1998)0022.3.co;2.
Moramarco, T., Barbetta, S., Bjerklie, D.M., Fulton, J.W., Tarpanelli, A., 2019. River bathymetry estimate and discharge assessment from remote sensing. Water Resour. Res. 55, 6692–6711.
Muste, M., Fujita, I., Hauet, A., 2008. Large-scale particle image velocimetry for measurements in riverine environments. Water Resour. Res. 44, W00D19. https://doi.org/10.1029/2008WR006950.
Muste, M., Lee, K., Kim, D., Bacotiu, C., Oliveros, M.R., Cheng, Z., Quintero, F., 2020. Revisiting hysteresis of flow variables in monitoring unsteady streamflows. J. Hydraul. Res. 58 (6), 867–887. https://doi.org/10.1080/00221686.2020.1786742.
NOAA (National Oceanic and Atmospheric Administration), 2019. Data Tools: Local Climatological Data (LCD). Local Climatological Data (LCD) | Data Tools | Climate Data Online (CDO) | National Climatic Data Center (NCDC). Retrieved July 10, 2019, from https://www.ncdc.noaa.gov/cdo-web/datatools/lcd.
NWS (National Weather Service), 2020. Normal Depth Demonstration Tool. Normal Depth Calculator. Retrieved February 21, 2020, from https://www.weather.gov/aprfc/NormalDepthCalc.
Plant, W.J., Keller, W.C., Hayes, K., 2005. Measurement of river surface currents with coherent microwave systems. IEEE Trans. Geosci. Remote Sens. 43 (6), 1242–1257.
Polatel, C., 2006. Large-scale roughness effect on free-surface and bulk flow characteristics in open-channel flows (Doctoral dissertation. University of Iowa).
PRISM, 2004. PRISM Climate Group, Oregon State University, http://prism.oregonstate.edu, created 4 Feb 2004.
Rantz, S. E., 1982. Measurement and computation of streamflow: Volume 1, Measurement of stage and discharge. U.S. Geological Survey Water Supply Paper 2175.
Rowinski, P.M., Czernuszenko, W., Marc, J.-M., 2000. Time-dependent shear velocities in channel routing. Hydrol. Sci. J. 45 (6), 881–895. https://doi.org/10.1080/02626660009492390.
Servat, E., Dezetter, A., 1991. Selection of calibration objective fonctions in the context of rainfall-ronoff modelling in a Sudanese savannah area. Hydrol. Sci. J. 36 (4), 307–330.
GmbH, S., 2014. Discharge Measurement System for RQ-30, RQ-30a Firmware version 1.8x: User Manual (V02). Author, Koblach, Austria.
Sun, X., Shiono, K., Chandler, J.H., Rameshwaran, P., Sellin, R.H.J., Fujita, I., 2010. Discharge estimation in small irregular river using LSPIV. In: Proceedings of the Institution of Civil Engineers-Water Management, pp. 247–254.
Tauro, F., Piscopia, R., Grimaldi, S., 2017. Streamflow observations from cameras: Large-scale particle image velocimetry or particle tracking velocimetry? Water Resour. Res. 53 (12), 10374–10394.
USGS (U.S. Geological Survey) (2020). TNM Download (V1.0), The National Map. Retrieved February 02, 2020, from https://viewer.nationalmap.gov/basic/.
Welber, M., Le Coz, J., Laronne, J.B., Zolezzi, G., Zamler, D., Dramais, G., Hauet, A., Salvaro, M., 2016. Field assessment of noncontact stream gauging using portable surface velocity radars (SVR). Water Resour. Res. 52 (2), 1108–1126. https://doi.org/10.1002/2015WR017906.